



ELSEVIER

Applied Mathematics and Computation 127 (2002) 23–43

APPLIED
MATHEMATICS
AND
COMPUTATION

www.elsevier.com/locate/amc

Finite element analysis of contaminant transport in groundwater

Tony W.H. Sheu ^{*}, Y.H. Chen

*Department of Naval Architecture and Ocean Engineering, National Taiwan University,
73 Chou-Shan Road, Taipei, Taiwan*

Abstract

In this paper, we focus on the development of a finite element model for predicting the contaminant concentration governed by the advective–dispersive equation. In this study, we take into account the first-order degradation of the contaminant to realistically model the transport phenomenon in groundwater. To solve the resulting unsteady advection–diffusion equation with production, a finite element model is constructed, which employs a quadratic basis function to approximate the contaminant concentration. The development of a weighted residuals finite element model involves constructing a biased test function to retain the scheme stability for wide ranges of values of the physical coefficients. In the process of constructing the Petrov–Galerkin finite element model for stability reasons, it is desirable to obtain an acceptable degree of accuracy. The method used to retain stability without loss of accuracy is to approximate the differential equation within the semi-discretization framework. After discretizing the time derivative term using the Euler time-stepping scheme, the resulting ordinary differential equation, which involves only the spatial derivative terms, is solved using the nodally exact finite element model. For better control of the user’s specified time step and mesh size, full analysis of the discretization scheme is conducted. In this study, both modified equation analysis and Fourier stability analysis are employed to better understand the proposed semi-discretized Petrov–Galerkin finite element model. Validation of the newly proposed model is accomplished through analysis of the results obtained for several test problems. Some of them are amenable to analytic solutions. The rate of convergence of the employed finite element model then can be obtained. © 2002 Elsevier Science Inc. All rights reserved.

^{*} Corresponding author.

E-mail address: tony.sheu@cf.na.ntu.edu.tw (T.W.H. Sheu).

Keywords: Advective–dispersive equation; First-order degradation; Petrov–Galerkin; Modified equation analysis; Fourier stability analysis

1. Introduction

The advective–dispersive equation characterizes the transport of contaminants in groundwater. Under many circumstances, reaction or degradation can play an essential role in the ensuing transport phenomena. As a result, the advective–dispersive transport equation with reaction has been the subject of much interest. The advent of faster computers with large core memories has allowed hydrogeologists to contemplate time-accurate simulation of contaminant transport. Up until very recently, mathematical models used to simulate contaminant transport in groundwater have proved to be useful for remedial design, in addition to risk assessment. It is this practical importance that motivated the present study.

Numerical investigations of the advective–dispersive equation have been quite plentiful. Comparatively few studies have focused on a more realistic advective–dispersive-reactive equation for modeling contaminant transport. Of the major methods developed for solving partial differential equations, the finite difference method seems to enjoy significant popularity, in particular in the early years because code implementation is easy. There are quite a few papers in the literature on this subject. A few we might mention are those of Ataie-Ashtiani et al. [1], Noye and Tan [2] and, more recently, Hossain [3].

The finite element method has also evolved significantly over the last few years. The ease of implementing Neumann-type boundary conditions and its capability of tackling complex geometries have made the finite element method particularly suitable for numerical simulation of transport equations. In addition, finite element method has a sound mathematical basis, which can be used to prove convergence of numerical solutions to the exact solution with mesh refinement. These desired features provided impetus for the present finite element simulation of contaminant transport in groundwater. In the literature, there exist papers dealing with the differential equation of present interest. Interested readers can refer to the works of Harari and Hughes [4], Hossain and Yonge [5,6], Idelsohn et al. [7], and Codina [8]. These references are by no means exhaustive, but they illustrate the popularity and wide use of finite element models to solve this class of problems.

It is well accepted that advective and reactive terms are the main causes leading to numerical instability. As a result, the utility of the finite element model depends to a large extent on the chosen weighting function. While the upwind finite element model is widely used in the fluid dynamic community,

the benefit of oscillation-free results is gained at the expense of significant numerical inaccuracy. A key goal in the present study is to obtain a more accurate solution. A pursuit of scheme stability and prediction accuracy is what motivated the present new development. Moreover, monotonic study of the scheme is made to provide support to show under what conditions the solution can retain a monotonic profile.

The remainder of this paper is organized as follows. In Section 2, we present the time-dependent differential equation, subject to initial and boundary conditions, for the contaminant transport. We then present the finite element model, which constitutes the main theme of the present study. The fundamentals of the newly proposed Petrov–Galerkin model will be also detailed. Both modified equation analysis and Fourier stability analysis are conducted to show in-depth the scheme's features. Section 5 is devoted to a monotonic study of the proposed scheme. The underlying theory is that of the M -matrix theory. As is usual, we provide evidence to show the applicability of the model to simulating the advective–dispersive–reactive model equation. In Section 7, we provide concluding remarks.

2. Working equation

Transport of contaminants in groundwater is primarily governed by advection and dispersion. In addition, reaction or degradation has an impact on the evolving transport of contaminants. In this light, we consider the following advective–dispersive equation with a first-order reaction or degradation. To simplify the description of the newly developed finite element model, we consider the following one-dimensional advection–diffusion–reaction (ADR) transport equation for the contaminant concentration C

$$\frac{\partial C}{\partial t} + u \frac{\partial C}{\partial x} = D \frac{\partial^2 C}{\partial x^2} - \lambda C. \quad (1)$$

In the above, u is the velocity, t the time, x the spatial coordinate, D the dispersion coefficient, and λ the decay constant. In order to make the above equation well posed, it is assumed that initial as well as boundary conditions are properly given a priori.

3. Finite element model

In this study, we seek solutions to Eq. (1) by applying the semi-discretization method. By doing so, time and spatial derivatives are approximated separately. Within the semi-discretization framework, the discretization of Eq. (1) begins with approximation of $\partial C/\partial t$ by means of

$$\frac{\partial C}{\partial t} = \frac{C^{n+1} - C^n}{\Delta t}. \quad (2)$$

The superscripts n and $n + 1$ represent two consecutive times t^n and t^{n+1} , with a time increment $\Delta t (\equiv t^{n+1} - t^n)$. Substitution of Eq. (2) into (1) yields

$$\bar{u} \frac{\partial C}{\partial x} = \bar{D} \frac{\partial^2 C}{\partial x^2} - \bar{\lambda} C + f, \quad (3)$$

where

$$\bar{u} = u \Delta t, \quad (4a)$$

$$\bar{D} = D \Delta t, \quad (4b)$$

$$\bar{\lambda} = 1 + \lambda \Delta t, \quad (4c)$$

$$f = C^n(x). \quad (4d)$$

The problem of finding C from the unsteady Eq. (1) is now transformed into that of finding the solution from the inhomogeneous steady-state Eq. (3) through the above semi-discretization approach.

It is then a question of constructing an appropriate spatial discretization of Eq. (3), which is akin to the following prototype equation for a passive scalar ϕ :

$$u \frac{\partial \phi}{\partial x} - k \frac{\partial^2 \phi}{\partial x^2} + \lambda \phi = f, \quad (5)$$

where f is allowed to vary with x . Spatial discretization of Eq. (5) is performed via the weighted residuals method, which is carried out on quadratic elements. The Petrov–Galerkin finite element, which is regarded as a refinement of its Galerkin counterparts, is chosen to obtain enhanced stability. In this paper, we take weighting functions \tilde{w}_i as the sum of shape function w_i and biased function P_i

$$\tilde{w}_i = w_i + P_i. \quad (6)$$

The Petrov–Galerkin models appropriate for solving Eq. (5) differ from each other in the choice of P_i . In this paper, P_i is chosen as

$$P_i = \alpha \frac{h}{2} w_i' + \gamma Q, \quad (7)$$

where the free parameters α and γ account for the advective and reactive contributions, respectively. In fact, the determination of α and γ is the core of the present study. In (7), h denotes the mesh size, and the superscript “'” represents the derivative notation. The two terms on the right-hand side of (7) are used for different purposes. The inclusion of first term originates from the idea of Hughes and Brooks [9]. The introduction of w_i' is known to be able to suppress oscillations in the analysis of convection–diffusion equation in cases where convection prevails. The purpose of adding the second term on the

right-hand side of Eq. (7) is to enhance stability when the reaction term dominates over other two effects [7].

Referring to Fig. 1, which shows quadratic elements, a linear polynomial Q is chosen because the polynomial degree for $\lambda\phi$ is only one order less than that of the diffusive term $-k(\partial^2\phi/\partial x^2)$ after the integration by parts is conducted on this term in the present weak formulation. For this reason, Q at the two end (or corner) nodes 1 and 3 are chosen as

$$Q_1 = -\frac{1}{2}(\xi - 1), \tag{8a}$$

$$Q_3 = \frac{1}{2}(1 + \xi). \tag{8b}$$

With the definitions of Q_1 and Q_3 , Q_2 at the center node can be chosen as the average of two corner values Q_1 and Q_3 . The reason is that the distance between nodes 1 and 2 is the same as that between nodes 2 and 3. For the above reason, Q_2 is chosen as

$$Q_2 = 1. \tag{9}$$

Having determined two finite element spaces, we can obtain the stiffness matrix equation and the source vector as in the conventional finite element method. On theoretical grounds, we must derive the corresponding algebraic equations, akin to those in the finite-difference equations, at corner and end nodes in quadratic elements. After some algebra, the discrete representations of the model Eq. (5) can be expressed. Due to a lack of space, we omit the detailed derivation but simply summarize the results as follows:

Corner node i in Fig. 1(a):

$$\begin{aligned} & \left(-\frac{8}{3} - \frac{4Pe}{3} + \frac{Rr}{15} - \frac{8Pe\alpha}{3} + \frac{Rr\alpha}{3} - 2Pe\gamma + \frac{Rr\gamma}{6} \right) \phi_{i-1} \\ & + \left(\frac{16}{3} + \frac{8Rr}{15} + \frac{16Pe\alpha}{3} + \frac{2Rr\gamma}{3} \right) \phi_i \\ & + \left(-\frac{8}{3} + \frac{4Pe}{3} + \frac{Rr}{15} - \frac{8Pe\alpha}{3} - \frac{Rr\alpha}{3} + 2Pe\gamma + \frac{Rr\gamma}{6} \right) \phi_{i+1} = f. \end{aligned} \tag{10}$$

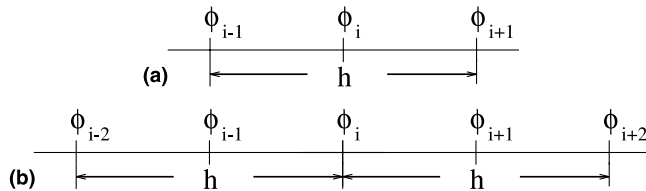


Fig. 1. The illustration of center and end nodes: (a) center node i ; (b) $i \pm 1$.

End nodes $i \pm 1$ in Fig. 1(b):

$$\begin{aligned}
 & \left(\frac{1}{3} + \frac{Pe}{3} - \frac{Rr}{30} - 2\alpha + \frac{Pe\alpha}{3} - \frac{Rr\alpha}{12} - \gamma - \frac{Pe\gamma}{3} \right) \phi_{i-2} \\
 & + \left(-\frac{8}{3} - \frac{4Pe}{3} + \frac{Rr}{15} + 4\alpha - \frac{8Pe\alpha}{3} + \frac{Rr\alpha}{3} - \frac{4Re\gamma}{3} + \frac{Pr\gamma}{3} \right) \phi_{i-1} \\
 & + \left(\frac{14}{3} + \frac{4Rr}{15} + \frac{14Pe\alpha}{3} + 2\gamma + \frac{Rr\gamma}{3} \right) \phi_i \\
 & + \left(-\frac{8}{3} + \frac{4Pe}{3} + \frac{Rr}{15} - 4\alpha - \frac{8Pe\alpha}{3} - \frac{Rr\alpha}{3} + \frac{4Re\gamma}{3} + \frac{Pr\gamma}{3} \right) \phi_{i+1} \\
 & + \left(\frac{1}{3} - \frac{Pe}{3} - \frac{Rr}{30} + 2\alpha + \frac{Pe\alpha}{3} + \frac{Rr\alpha}{12} - \gamma + \frac{Pe\gamma}{3} \right) \phi_{i+2} = f. \quad (11)
 \end{aligned}$$

where

$$Pe = \frac{uh}{2k}, \quad (12)$$

$$Rr = \frac{\lambda h^2}{k}. \quad (13)$$

At this point, the solutions are amenable to algebraic calculations provided that α and γ are given. This is the main theme of the present study since they alone determine the solution quality. We obtain a higher level of prediction accuracy by taking the following general solution of Eq. (5) into account

$$\phi_{\text{exact}} = ae^{m_1x} + be^{m_2x}. \quad (14)$$

In the above, a and b are two constants. As for m_1 and m_2 , they are derived as follows by substituting (14) into Eq. (5)

$$m_1 = \frac{u}{2k} + \left[\left(\frac{u}{2k} \right)^2 + \frac{\lambda}{k} \right]^{1/2}, \quad (15)$$

$$m_2 = \frac{u}{2k} - \left[\left(\frac{u}{2k} \right)^2 + \frac{\lambda}{k} \right]^{1/2}. \quad (16)$$

Substitution of the analytic values of ϕ_i , $\phi_{i \pm 1}$, and $\phi_{i \pm 2}$ into the algebraic Eqs. (10) and (11) enables us to determine the nodally exact expressions of α and γ , which are detailed in Appendix A. The representations of α and γ are mathematically very complex in form. Therefore, it is instructive to plot them graphically. Figs. 2 and 3 plot α and γ against the dimensionless variables Pe and Rr , as defined in Eqs. (12) and (13). Upon obtaining the analytic expressions of α and γ , the formulation of the finite element model is completed.

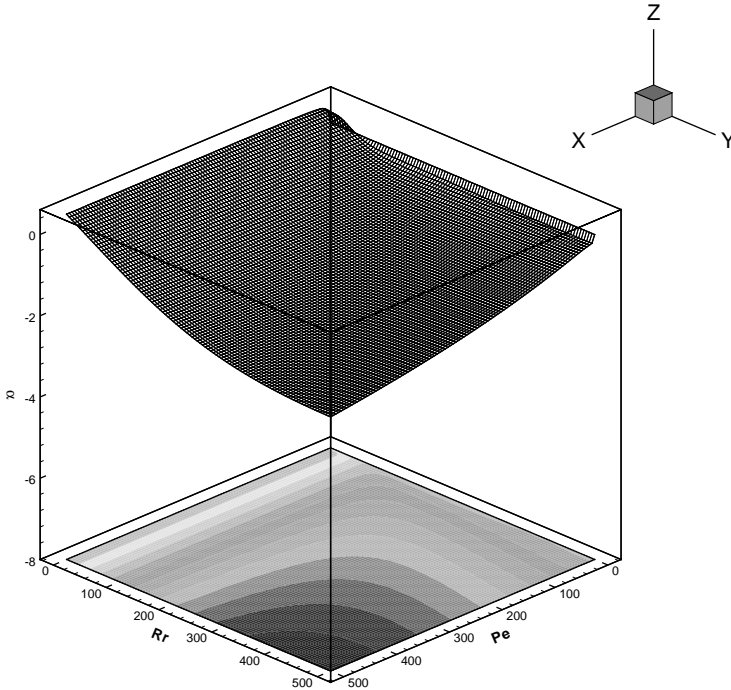


Fig. 2. The plot of α against Pe and Rr .

4. Fundamental study of the model equation

In order to shed light on the nature of the proposed ADR scheme, we will conduct modified equation analysis [10]. Substituting Taylor-series expansions into Eqs. (10) and (11) for ϕ_{i+1}^{n+1} , ϕ_{i-1}^{n+1} and ϕ_i^n , we can obtain the modified equation of the first kind. At corner and end nodes, these modified equations are derived, respectively, as

Center node:

$$\begin{aligned} \phi_t + u\phi_x - k\phi_{xx} + \lambda\phi - f &= \left(\frac{\Delta t \lambda^2}{2} - \frac{\Delta t^2 \lambda^3}{3} + \frac{\Delta t^3 \lambda^4}{6} \right) \phi \\ &+ \left(u\Delta t \lambda - u\Delta t^2 \lambda^2 + \frac{2u\Delta t^3 \lambda^3}{3} - \frac{hu\alpha\Delta t \lambda^2 (3 - 2\Delta t \lambda + \Delta t^2 \lambda^2)}{6(2 + 3\gamma)} \right) \phi_x \\ &+ \left(\frac{-3k\gamma}{2 + 3\gamma} + \frac{u^2 \Delta t}{2} - \frac{2k\Delta t \lambda}{2 + 3\gamma} - \frac{hu\alpha\Delta t \lambda}{2 + 3\gamma} - u^2 \Delta t^2 \lambda + \frac{h^2 \Delta t \lambda^2}{20(2 + 3\gamma)} - \frac{h^2 \gamma \Delta t \lambda^2}{8(2 + 3\gamma)} \right) \phi_{xx} \end{aligned}$$

$$\begin{aligned}
& + \frac{k\Delta t^2 \lambda^2}{2+3\gamma} + \frac{hu\alpha\Delta t^2 \lambda^2}{2(2+3\gamma)} + \frac{3k\gamma\Delta t^2 \lambda^2}{2(2+3\gamma)} + \frac{2u^2\Delta t^3 \lambda^2}{2+3\gamma} + \frac{3u^2\gamma\Delta t^3 \lambda^2}{2+3\gamma} - \frac{k\Delta t^3 \lambda^3}{2+3\gamma} \\
& - \frac{hu\alpha\Delta t^3 \lambda^3}{2(2+3\gamma)} - \frac{3k\gamma\Delta t^3 \lambda^3}{2(2+3\gamma)} \Big) \phi_{xx} + \left(\frac{-h^2u}{30(2+3\gamma)} + \frac{hk\alpha}{2+3\gamma} - \frac{2ku\Delta t}{2+3\gamma} \right. \\
& - \frac{hu^2\alpha\Delta t}{2(2+3\gamma)} - \frac{u^3\Delta t^2}{3} + \frac{2h^2u\Delta t\lambda}{15(2+3\gamma)} + \frac{h^2u\gamma\Delta t\lambda}{4(2+3\gamma)} + \frac{2ku\Delta t^2\lambda}{2+3\gamma} + \frac{3ku\gamma\Delta t^2\lambda}{2+3\gamma} \\
& + \frac{4u^3\Delta t^3\lambda}{3(2+3\gamma)} + \frac{2u^3\gamma\Delta t^3\lambda}{2+3\gamma} - \frac{h^3\alpha\Delta t\lambda^2}{24(2+3\gamma)} - \frac{hk\alpha\Delta t^2\lambda^2}{2(2+3\gamma)} - \frac{3ku\Delta t^3\lambda^2}{2+3\gamma} \\
& \left. - \frac{hu^2\alpha\Delta t^3\lambda^2}{2(2+3\gamma)} - \frac{9ku\gamma\Delta t^3\lambda^2}{2(2+3\gamma)} + \frac{hk\alpha\Delta t^3\lambda^3}{2(2+3\gamma)} \right) \phi_{xxx} + \text{H.O.T.} \tag{17}
\end{aligned}$$

End node:

$$\begin{aligned}
\phi_t + u\phi_x - k\phi_{xx} + \lambda\phi - f & = \left(\frac{\Delta t\lambda^2}{2} - \frac{\Delta t^2\lambda^3}{3} + \frac{\Delta t^3\lambda^4}{6} \right) \phi \\
& + \left(u\Delta t\lambda - \frac{h\alpha\Delta t\lambda^2}{4(1+3\gamma)} - u\Delta t^2\lambda^2 + \frac{h\alpha\Delta t^2\lambda^3}{6(1+3\gamma)} + \frac{2u\Delta t^3\lambda^3}{3} - \frac{h\alpha\Delta t^3\lambda^4}{12(1+3\gamma)} \right) \phi_x \\
& + \left(\frac{u^2\Delta t}{2} - k\Delta t\lambda - \frac{hu\alpha\Delta t\lambda}{2(1+3\gamma)} - u^2\Delta t^2\lambda - \frac{h^2\Delta t\lambda^2}{40(1+3\gamma)} + \frac{h^2\gamma\Delta t\lambda^2}{8(1+3\gamma)} \right. \\
& + k\Delta t^2\lambda^2 + \frac{hu\alpha\Delta t^2\lambda^2}{2(1+3\gamma)} + u^2\Delta t^3\lambda^2 + \frac{h^2\Delta t^2\lambda^3}{40(1+3\gamma)} - \frac{h^2\gamma\Delta t^2\lambda^3}{8(1+3\gamma)} - \frac{k\Delta t^3\lambda^3}{2} \\
& \left. - \frac{hu\alpha\Delta t^3\lambda^3}{4(1+3\gamma)} \right) \phi_{xx} + \left(\frac{h^2u}{30(1+3\gamma)} - \frac{hk\alpha}{1+3\gamma} - ku\Delta t - \frac{hu^2\alpha\Delta t}{4(1+3\gamma)} - \frac{u^3\Delta t^2}{3} \right. \\
& - \frac{h^2u\Delta t\lambda}{12(1+3\gamma)} + \frac{3hk\alpha\Delta t\lambda}{2(1+3\gamma)} + \frac{h^2u\gamma\Delta t\lambda}{4(1+3\gamma)} + 2ku\Delta t^2\lambda + \frac{hu^2\alpha\Delta t^2\lambda}{2(1+3\gamma)} + \frac{2u^3\Delta t^3\lambda}{3(1+3\gamma)} \\
& + \frac{2u^3\gamma\Delta t^3\lambda}{1+3\gamma} + \frac{h^3\alpha\Delta t\lambda^2}{24(1+3\gamma)} + \frac{h^2u\Delta t^2\lambda^2}{20(1+3\gamma)} - \frac{hk\alpha\Delta t^2\lambda^2}{4(1+3\gamma)} - \frac{h^2u\gamma\Delta t^2\lambda^2}{4(1+3\gamma)} \\
& \left. - \frac{3ku\Delta t^3\lambda^2}{2(1+3\gamma)} - \frac{hu^2\alpha\Delta t^3\lambda^2}{4(1+3\gamma)} - \frac{9ku\gamma\Delta t^3\lambda^2}{2(1+3\gamma)} + \frac{hk\alpha\Delta t^3\lambda^3}{4(1+3\gamma)} \right) \phi_{xxx} + \text{H.O.T.} \tag{18}
\end{aligned}$$

Note that the left-hand side Eqs. (17) and (18) correspond to the investigated model equation. As for the terms on the right-hand side of these equations, they represent the discretization errors. Having derived Eqs. (17) and (18), it is clear that the consistency property that is necessary to obtain a convergent solution is achieved as Δt and h approach zero.

As a fundamental study of the proposed scheme, we will also consider Fourier (or von Neumann) stability analysis for Eqs. (10) and (11). First, we can derive the amplification factor for this scheme by conducting standard stability analysis. Let $\beta = (2\pi m/2L)h$ ($m = 0, 1, 2, 3, \dots, M$), let h be the mesh

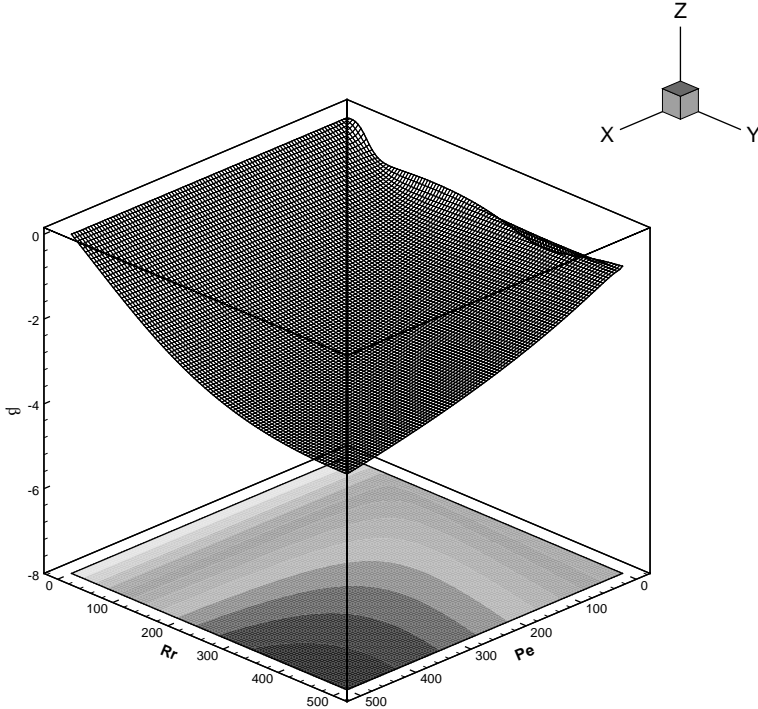


Fig. 3. The plot of γ against Pe and Rr .

size, and let $2L$ be the period of the fundamental frequency ($m = 1$); the amplification factor

$$|G| \left(\equiv \left| \frac{\phi_j^{n+1}}{\phi_j^n} \right| \right)$$

is derived as

$$G = \frac{A}{B}, \tag{19}$$

$$|G| = \sqrt{\text{Im}(G)^2 + \text{Re}(G)^2}, \tag{20}$$

where A and B at the center and end nodes are expressed, respectively, as follows:

Center node:

$$A = TH \left((2 + 5\gamma) \cos \left(\frac{hk_x}{2} \right) + 2 \left(4 + 5\gamma - 5i\alpha \sin \left(\frac{hk_x}{2} \right) \right) \right), \tag{21}$$

$$\begin{aligned}
B = & (-80 + 2TH - 40CX\beta + 5TH\gamma + RX(2 + 5\gamma)) \cos\left(\frac{hk_x}{2}\right) \\
& + 2\left(40 + 4RX + 4TH + 20CX\beta + 5RX\gamma + 5TH\gamma \right. \\
& \left. + 5i(2CX - RX\beta - TH\beta + 3CX\gamma) \sin\left(\frac{hk_x}{2}\right)\right). \quad (22)
\end{aligned}$$

End node:

$$\begin{aligned}
A = TH & \left(8 + 10\gamma + 4(1 + 5\gamma) \cos\left(\frac{hk_x}{2}\right) - 2 \cos(hk_x) \right. \\
& \left. - 20i\beta \sin\left(\frac{hk_x}{2}\right) + 5i\beta \sin(hk_x)\right), \quad (23)
\end{aligned}$$

$$\begin{aligned}
B = 140 + 8RX + 8TH + 70CX\beta + 60\gamma + 10RX\gamma + 10TH\gamma \\
+ 4(-40 + RX + TH - 20CX\beta + 5RX\gamma + 5TH\gamma) \cos\left(\frac{hk_x}{2}\right) \\
- 2(-10 + RX + TH - 5CX\beta + 30\gamma) \cos(hk_x) \\
+ 20i((-12 - RX - TH)\beta + 2CX(1 + \gamma)) \sin\left(\frac{hk_x}{2}\right) \\
+ 5i((24 + RX + TH)\beta + 2CX(-1 + \gamma)) \sin(hk_x). \quad (24)
\end{aligned}$$

In the above,

$$CX = \frac{uh}{k}, \quad RX = \frac{\lambda h^2}{k}, \quad \text{and} \quad TH = \frac{h^2}{\Delta tk}.$$

From Eq. (20), it is clear that the finite element model proposed here is unconditionally stable. By the Lax equivalent theorem [11], the solutions obtained from Eqs. (10) and (11) are indeed convergent.

The amplification factor shown in (19) can be rewritten in its exponential form as $G = |G| e^{i\theta}$, where θ denotes the phase angle

$$\theta = \tan^{-1} \left| \frac{\text{Im}(G)}{\text{Re}(G)} \right|. \quad (25)$$

To study how the phase angle θ varies with Pe , Rr and the other important dimensionless number,

$$v = \frac{u\Delta t}{h}, \quad (26)$$

we must derive the exact phase angle θ_e .

With the derived exact phase angle $\theta_e = -v\beta$, we can obtain the following relative phase shift error over an arbitrary time increment

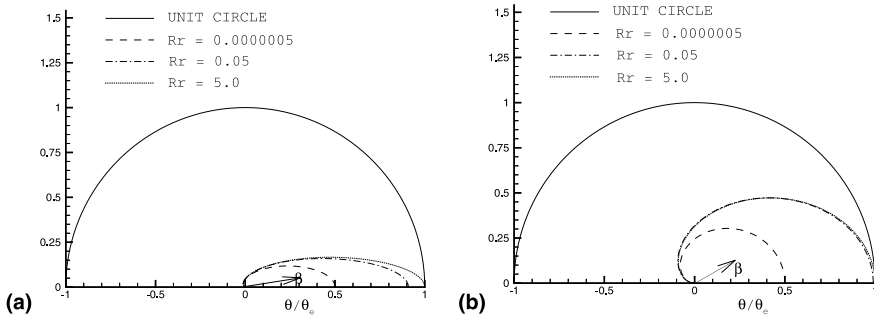


Fig. 4. The plot of θ/θ_c against Rr for two sets of values ν and Pe : (a) $Pe = 0.25, \nu = 1.0$; (b) $Pe = 0.25, \nu = 0.1$.

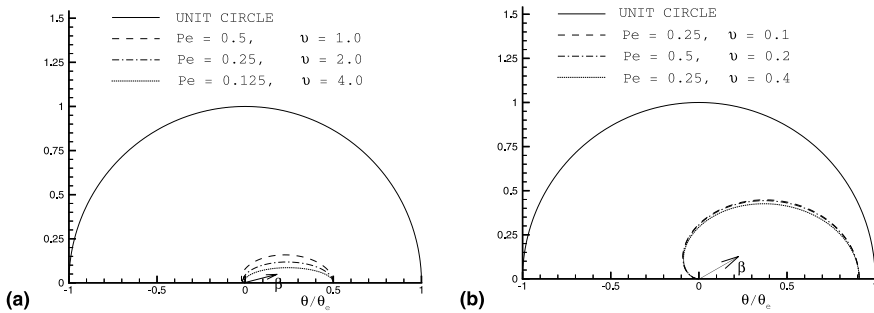


Fig. 5. The plot of θ/θ_c against Pe and ν for a fixed value of Rr : (a) $Rr = 0.5$; (b) $Rr = 0.5$.

$$\frac{\theta}{\theta_c} = \frac{\tan^{-1} |\text{Im}(G)/\text{Re}(G)|}{-\nu\beta}. \tag{27}$$

We plot θ/θ_c against Pe, Rr and β in Figs. 4 and 5. When the relative phase error exceeds a value of 1 for the specified values of Pe, Rr and β , the numerical solution has a wave speed greater than the exact wave speed, and this is called a phase-leading error. Otherwise the error is called a lagging phase error.

5. Monotonicity for the finite element equations

Besides consistency and stability properties that are two important ingredients for obtaining convergent solutions, the solution monotonicity property is also important for the development of an effective finite element model. Therefore, another key task in the current study is to determine the ranges of grid sizes h and time steps Δt that allow us to compute monotonic solutions

under the given values of u , k and λ . The key here to guaranteeing that monotonic solutions will be obtained is the use of the theory of the M -matrix [12–14]. According to [13], an implicit scheme given by Eqs. (10) and (11), or more compactly by $G(\phi^n) = \phi^{n-1}$, is said to be monotonic with time is that $\phi - \phi^* \geq 0$ if $G(\phi) - G(\phi^*) \geq 0$. Assume that we intend to advance the solution from t^{n-1} to t^n under the condition that $\phi^{n-1} - \phi^{n-2} \geq 0$; by definition, we have $\phi^{n-1} - \phi^{n-2} = G(\phi^n) - G(\phi^{n-1})$. The above condition for monotonicity in time can be analyzed by the concept of monotonic matrices and M -matrices. The reader is referred to [12,14] for additional details of the theory.

To clarify the underlying idea, let us define some useful definitions. The first definition concerns the M -matrix. A matrix is an M -matrix if and only if \underline{M} is classified as an L -matrix. In addition, it is required that there exist a diagonal matrix $\underline{D} = \text{diag}(d_i) \geq 0$ such that $\underline{D} \underline{M}$ is columnwise strictly diagonally dominant (i.e., $\sum_i a_{ij} d_i > 0$) or that $\underline{M} \underline{D}$ is rowwise strictly diagonally dominant (i.e., $\sum_j a_{ij} d_i > 0$) [13]. In the above, the matrix \underline{N} is an L -matrix if the splitting $\underline{N} = \underline{N}_1 - \underline{N}_2$, where $\underline{N}_1 = \text{diag}(b_i)$ is the diagonal matrix $b_i = n_{ii}$ and has the property $\underline{N}_1 \geq 0$ and $\underline{N}_2 \geq 0$. According to [13], the present implicit scheme is monotonic if the Jacobian $\partial \underline{G} / \partial \underline{\phi}$ is an M -matrix and, hence, the resulting matrix is monotonic. The implication is that if $\underline{A} \underline{\phi} \geq 0$, where the matrix \underline{A} contains components given in Eqs. (10) and (11), then $\underline{\phi} \geq 0$ holds.

Given the above definitions and theorem, the key to obtaining a monotonic solution ϕ , computed from Eqs. (10) and (11), is that $a_{ij} \leq 0$ for $i \neq j$, and that $|a_{ii}| \geq \sum_j |a_{ij}|$ for $(i \neq j)$. If this is the case, the matrix equation is, by definition, irreducible diagonally dominant. A matrix of this type is called an M -matrix, and $\underline{A}^{-1} > 0$ holds. Under this condition, the solutions computed from the M -matrix equation are monotonically distributed in the flow. Based on the M -matrix theory [12], there is a potential advantage in using the proposed scheme to resolve any possible sharp gradient in the flow. To show this, we can

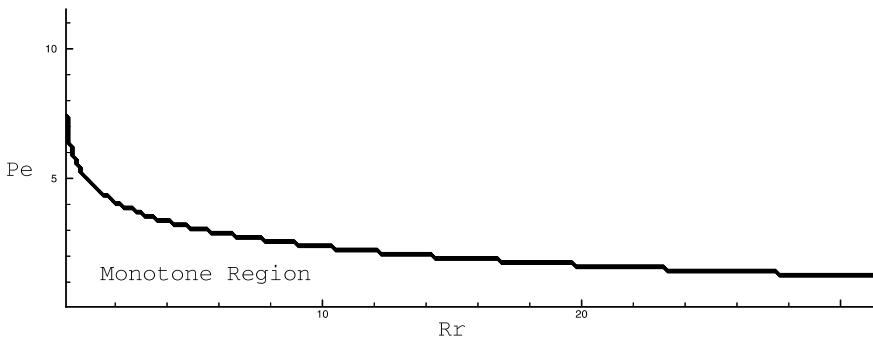


Fig. 6. An illustration of the monotonic region in the $(R_r - P_c)$ plot, where $P_c = uh/2k$ and $R_r = \lambda h^2/k$.

determine the monotonic region by varying the values of P_e and R_r , defined in Eqs. (12) and (13). As Fig. 6 shows, which plots the monotonic region against R_r and P_e , the solutions are unconditionally monotonic as long as the Peclet number defined in Eq. (12) falls below 0.5.

6. Numerical results

6.1. Validation study

As is always the case when a new scheme for solving the differential equation is presented, we need to validate our proposed scheme. For this purpose, we employed test problems which were amenable to analytic solutions. For Eq. (5), we considered first the homogeneous case where $f = 0$. To a first approximation, the coefficients u , k and c in this steady convection–diffusion–reaction equation, defined in the region $0 \leq x \leq 1$, were all assumed to be constant. Under these assumptions, the exact solution for (5) has the following form

$$\phi_{\text{exact}} = \frac{g_0 \exp\left(\frac{ux}{2k}\right) \sin\left(\sqrt{\frac{\lambda}{k} + \frac{u^2}{4k^2}}(1-x)\right) + g_1 \exp\left(\frac{u(x-1)}{2k}\right) \sin\left(\sqrt{\frac{\lambda}{k} + \frac{u^2}{4k^2}}x\right)}{\sin\left(\sqrt{\frac{\lambda}{k} + \frac{u^2}{4k^2}}\right)}. \tag{28}$$

The solution was obtained under boundary conditions specified as $\phi(0) = g_0 = 10$ and $\phi(1) = g_1 = -1$. We considered the uniform grid case with $h = 1/20$ and plot the computed result, for the case with $k = 4$, $u = 4$ and $\lambda = 100$, in Fig. 7. It is found to reproduce the analytic solution of the test equation. This test verifies that the proposed finite-element model can provide a nodally exact steady-state solution.

Having validated the code against the above one-dimensional homogeneous test problem, our attention is now drawn to the inhomogeneous case where $f = x^2(4x - 1)$. To verify the level of accuracy and allow comparison with the analytic solution, we considered a second test problem which involved variable coefficients $k = x^2$, $u = x$ and $c = 1$. Subject to the Dirichlet-type boundary condition, the exact solution to the inhomogeneous variable convection–diffusion–reaction equation was derived as

$$\phi_{\text{exact}} = (1-x)x^2. \tag{29}$$

Uniform grids were overlaid on the region $0.2 \leq x \leq 2.0$. The results were computed under $h = 0.09$ and are plotted in Fig. 8. Comparison shows good agreement with the exact solutions given in (31), thus demonstrating the

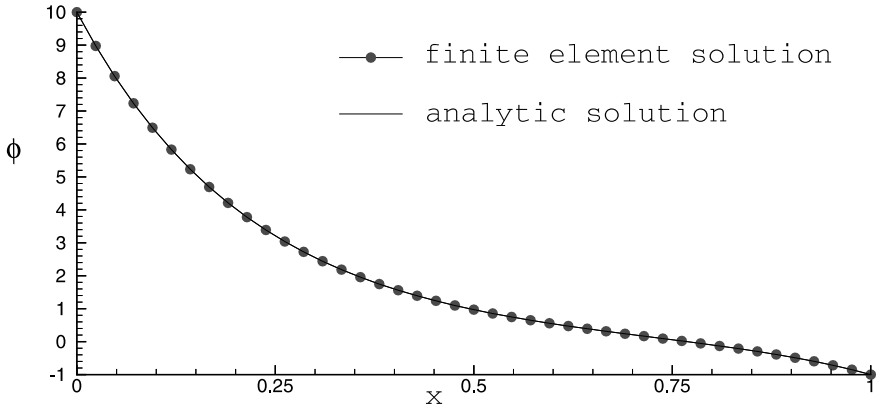


Fig. 7. A comparison of the finite element solution and the analytic solution, given in Eq. (28), for the homogeneous model equation.

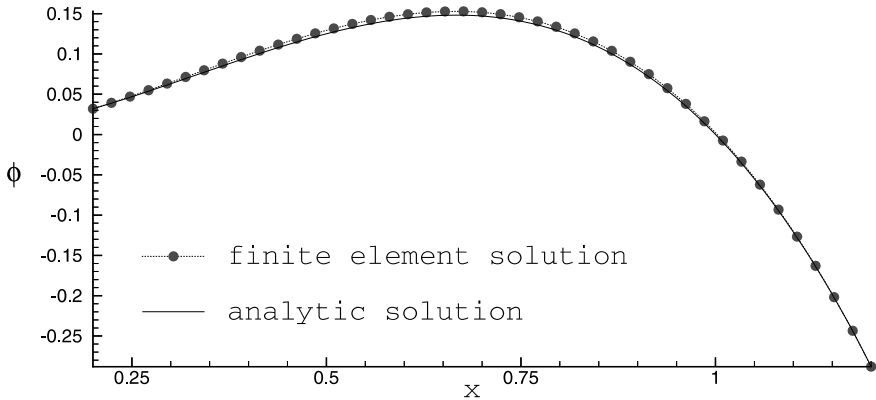


Fig. 8. A comparison of the finite element solution and the analytic solution, given in Eq. (29), for the inhomogeneous model equation.

applicability of the proposed model to solving the inhomogeneous ADR equation.

Having verified the applicability of the proposed scheme to steady-state analyses, we now turn our attention to the transient convection–diffusion–reaction equation in a unit domain of $0 \leq x \leq 1$

$$\phi_t + u\phi_x - k\phi_{xx} + \lambda\phi = f, \quad (30)$$

where $f = 2(x - 1)e^{-t}$. We started the calculation at $t = 0$ with the initial data $\phi(x, t = 0) = x^2$. The exact solution for the case with $u = 1$, $\lambda = 1$ and $k = 1$ takes the following form

$$\phi_{\text{exact}}(x, t) = x^2 e^{-t}. \quad (31)$$

Under the conditions $\Delta t = 5 \times 10^{-2}$ and $h = 0.05$, the computed solution at $t = 1$ agrees well with the exact solution plotted in Fig. 9, with the L_2 -error norm computed as 0.115808×10^{-4} . We also carried out computations on continuously refined grids with $h = \frac{1}{2}, \frac{1}{4}, \frac{1}{8}, \frac{1}{16}, \frac{1}{32}$ and computed prediction errors in their L_2 -norms. This was followed by plotting $\log(\text{err}_1/\text{err}_2)$ against $\log(h_1/h_2)$ for the errors err_1 and err_2 computed at two continuously refined grids h_1 and h_2 . As Fig. 10 shows, the rate of convergence obtained is 1.827703 using the proposed scheme.

6.2. Contaminant transport in groundwater

With reasonable confidence of investigating three tests which were amenable to exact solutions, we next tested a more stringent problem. A schematic of the test problem is shown in Fig. 11, which shows a sharp change in slope of the initial concentration $C(x, t = 0)$. As a test problem designed to demonstrate the ability of the code to capture sharply varying evolution of the contaminant concentrations, we considered a flow velocity of 2 m day^{-1} in a domain of 100 m. The mesh size is chosen to be $h = 1 \text{ m}$. Based on a timestep of $5 \times 10^{-2} \text{ day}$, the resulting Courant number obtained was 10^{-3} . As for the dispersion coefficient D , it was chosen as $0.1 \text{ m}^2 \text{ day}^{-1}$. The calculation was performed at the decay constant is $5 \times 10^{-2} \text{ day}^{-1}$. Under these conditions, the solutions were computed based on the dimensionless parameters $P_e = 5$, $R_r = 0.00625$ and $\nu = 0.25$. In this case, P_e and R_r are both within the monotonic region shown in Fig. 6. A schematic of the concentration profile and its subsequent evolution

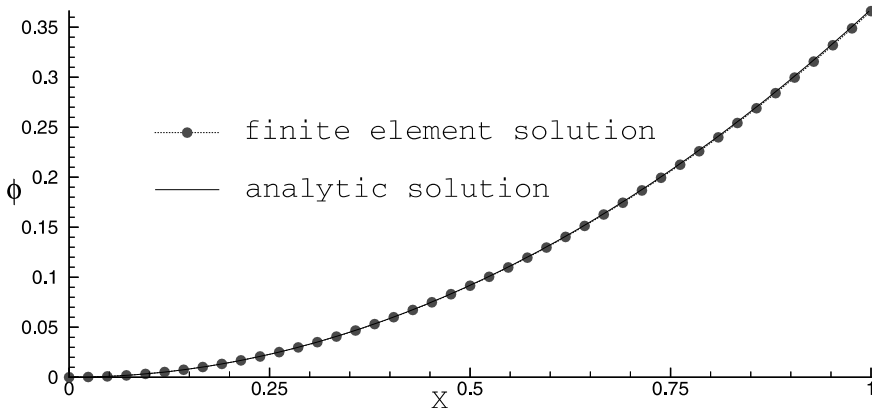


Fig. 9. A comparison of the finite element solution and the analytic solution, given in Eq. (31), for the transient problem.

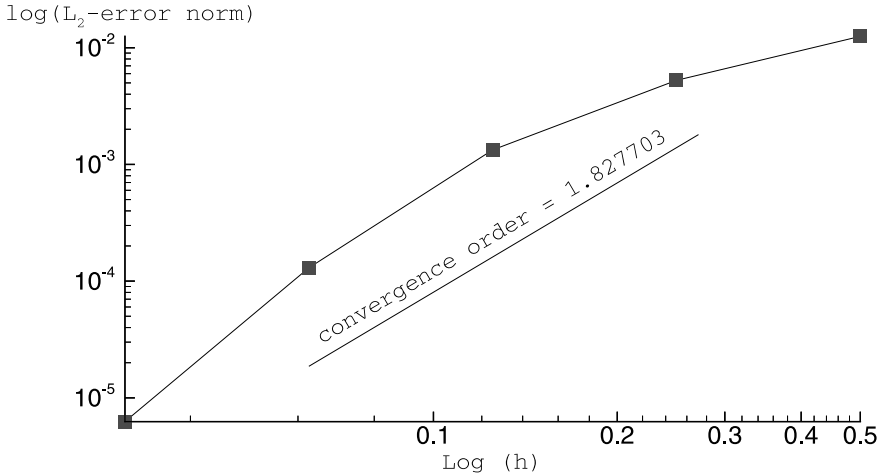


Fig. 10. The rate of convergence of this finite element scheme. $\log(L_2 - \text{error norms})$ is plotted against $\log(\Delta x)$.

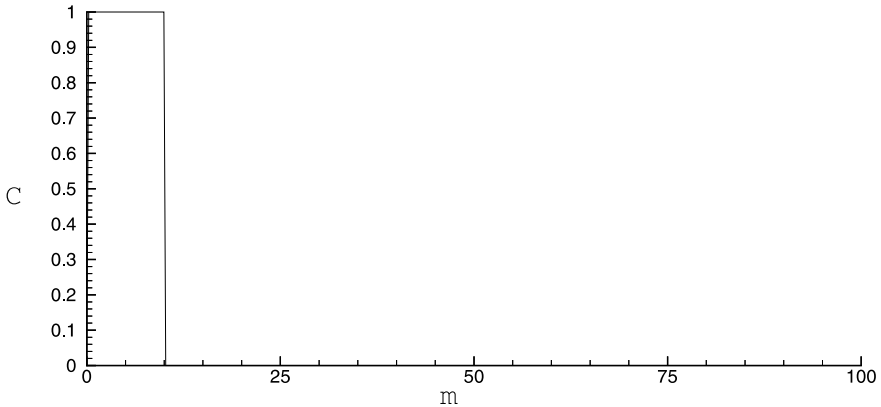
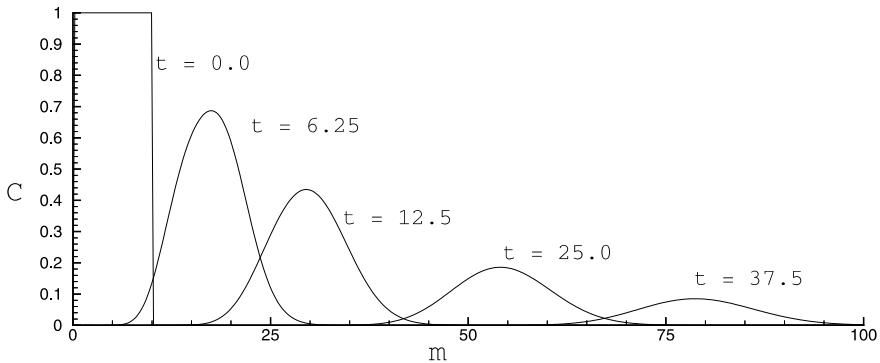


Fig. 11. The schematic of the initial profile.

are shown in Fig. 12. Evidence that the scheme has the ability to provide a monotonic solution can be seen since no oscillatory solutions of C are shed downstream of the incoming flow. This striking observation is true over the entire range of the monotonic region shown schematically in Fig. 6.

To further support the above numerical observations, we offer another means, namely, total variation (TV) analysis of the computed data. This analysis demands that the TV of a physically possible solution of C does not increase in time. By definition, the TV of the discrete system is

Fig. 12. The change of concentration C with time.

$$\text{TV}(C) = \sum_j |C_{j+1} - C_j|. \quad (32)$$

Following the work of Harten [15], we consider the numerical model to be TV diminishing (TVD) if

$$\text{TV}(C^{n+1}) \leq \text{TV}(C^n). \quad (33)$$

Given the above TVD condition, the computed solution indeed satisfies Eq. (33). Thus, the present computed solutions show no tendency to be oscillatory provided that the flow velocity, fluid viscosity, mesh size, and timestep, altogether, fall within the monotonic region.

7. Concluding remarks

In this work, we have proposed and analyzed a finite element method for solving the problem of contaminant concentration governed by the unsteady advection–dispersion equation with linear degradation in one dimension. To design a finite element model that solves the advective–dispersive–reactive transport equation for a passive scalar, we have formulated the problem within the semi-discretization context. Employing quadratic shape functions, we find that the Petrov–Galerkin finite element model for approximating spatial derivatives provides a nodally exact solution for the resulting ordinary differential equation. Our goals of pursuing good stability and high level of accuracy have, thus, been achieved. The analysis of this model has been placed on a rigorous analytic foundation. To obtain an in-depth understanding of the model presented here, we have conducted modified equation analysis and Fourier stability analysis. Based on the Lax equivalent theorem, the convergence of the solution to an exact one is, thus, expected

when meshes are continuously refined. The results obtained have a much greater range of validity in the sense that no oscillations are observed in circumstances in which advection becomes dominant over other competing terms.

Acknowledgements

Financial support for this research was provided by the NSC, R.O.C., under Grant NSC 88-2611-E-002-025.

Appendix A

The expressions of α and γ shown in Eq. (7) are, respectively, as follows:
Center node:

$$\alpha = \frac{AA}{CC}, \quad (\text{A.1})$$

$$\gamma = \frac{BB}{CC}, \quad (\text{A.2})$$

where

$$AA = -2(-60 + Rr)(-4Pe \cosh(a) + 4Pe \cosh(b) + Rr \sinh(a)), \quad (\text{A.3})$$

$$BB = -8(40Pe^2 + (-10 + Rr)Rr) \cosh(a) - 2(-160Pe^2 + 40Rr + Rr^2) \cosh(b) + 80PeRr \sinh(a), \quad (\text{A.4})$$

$$CC = 5(2(48Pe^2 + Rr^2) \cosh(a) + (-96Pe^2 + Rr^2) \cosh(b) - 24PeRr \sinh(a)). \quad (\text{A.5})$$

End node:

$$\alpha = \frac{BE - AF}{DE + CF}, \quad (\text{A.6})$$

$$\gamma = -\frac{BC - AD}{DE + CF}, \quad (\text{A.7})$$

where

$$\begin{aligned}
 A = & \frac{14}{3} - \frac{4Rr}{15} - \frac{16 \cosh\left(\frac{ah}{2}\right) \cosh\left(\frac{bh}{2}\right)}{3} - \frac{2Rr \cosh\left(\frac{ah}{2}\right) \cosh\left(\frac{bh}{2}\right)}{15} \\
 & + \frac{2 \cosh\left(\frac{ah}{2}\right)^2 \cosh\left(\frac{bh}{2}\right)^2}{3} + \frac{Rr \cosh\left(\frac{ah}{2}\right)^2 \cosh\left(\frac{bh}{2}\right)^2}{15} \\
 & + \frac{8Pe \cosh\left(\frac{bh}{2}\right) \sinh\left(\frac{ah}{2}\right)}{3} - \frac{4Pe \cosh\left(\frac{ah}{2}\right) \cosh\left(\frac{bh}{2}\right) \sinh\left(\frac{ah}{2}\right)}{3} \\
 & + \frac{2 \cosh\left(\frac{bh}{2}\right)^2 \sinh\left(\frac{ah}{2}\right)^2}{3} + \frac{Rr \cosh\left(\frac{bh}{2}\right)^2 \sinh\left(\frac{ah}{2}\right)^2}{15} \\
 & + \frac{2 \cosh\left(\frac{ah}{2}\right)^2 \sinh\left(\frac{bh}{2}\right)^2}{3} + \frac{Rr \cosh\left(\frac{ah}{2}\right)^2 \sinh\left(\frac{bh}{2}\right)^2}{15} \\
 & - \frac{4Pe \cosh\left(\frac{ah}{2}\right) \sinh\left(\frac{ah}{2}\right) \sinh\left(\frac{bh}{2}\right)^2}{3} + \frac{2 \sinh\left(\frac{ah}{2}\right)^2 \sinh\left(\frac{bh}{2}\right)^2}{3} \\
 & + \frac{Rr \sinh\left(\frac{ah}{2}\right)^2 \sinh\left(\frac{bh}{2}\right)^2}{15}, \tag{A.8}
 \end{aligned}$$

$$\begin{aligned}
 B = & \frac{8Pe \cosh\left(\frac{ah}{2}\right) \sinh\left(\frac{bh}{2}\right)}{3} - \frac{4Pe \cosh\left(\frac{ah}{2}\right)^2 \cosh\left(\frac{bh}{2}\right) \sinh\left(\frac{bh}{2}\right)}{3} \\
 & - \frac{16 \sinh\left(\frac{ah}{2}\right) \sinh\left(\frac{bh}{2}\right)}{3} - \frac{2Rr \sinh\left(\frac{ah}{2}\right) \sinh\left(\frac{bh}{2}\right)}{15} \\
 & + \frac{8 \cosh\left(\frac{ah}{2}\right) \cosh\left(\frac{bh}{2}\right) \sinh\left(\frac{ah}{2}\right) \sinh\left(\frac{bh}{2}\right)}{3} \\
 & + \frac{4Rr \cosh\left(\frac{ah}{2}\right) \cosh\left(\frac{bh}{2}\right) \sinh\left(\frac{ah}{2}\right) \sinh\left(\frac{bh}{2}\right)}{15} \\
 & - \frac{4Pe \cosh\left(\frac{bh}{2}\right) \sinh\left(\frac{ah}{2}\right)^2 \sinh\left(\frac{bh}{2}\right)}{3}, \tag{A.9}
 \end{aligned}$$

$$\begin{aligned}
 C = & \frac{14Pe}{3} - \frac{16Pe \cosh\left(\frac{ah}{2}\right) \cosh\left(\frac{bh}{2}\right)}{3} + \frac{2Pe \cosh\left(\frac{ah}{2}\right)^2 \cosh\left(\frac{bh}{2}\right)^2}{3} \\
 & - 8 \cosh\left(\frac{bh}{2}\right) \sinh\left(\frac{ah}{2}\right) + \frac{2Rr \cosh\left(\frac{bh}{2}\right) \sinh\left(\frac{ah}{2}\right)}{3} \\
 & + 8 \cosh\left(\frac{ah}{2}\right) \cosh\left(\frac{bh}{2}\right)^2 \sinh\left(\frac{ah}{2}\right) \\
 & - \frac{Rr \cosh\left(\frac{ah}{2}\right) \cosh\left(\frac{bh}{2}\right)^2 \sinh\left(\frac{ah}{2}\right)}{3} + \frac{2Pe \cosh\left(\frac{bh}{2}\right)^2 \sinh\left(\frac{ah}{2}\right)^2}{3}
 \end{aligned}$$

$$\begin{aligned}
& + \frac{2Pe \cosh\left(\frac{ah}{2}\right)^2 \sinh\left(\frac{bh}{2}\right)^2}{3} + 8 \cosh\left(\frac{ah}{2}\right) \sinh\left(\frac{ah}{2}\right) \sinh\left(\frac{bh}{2}\right)^2 \\
& - \frac{Rr \cosh\left(\frac{ah}{2}\right) \sinh\left(\frac{ah}{2}\right) \sinh\left(\frac{bh}{2}\right)^2}{3} + \frac{2Pe \sinh\left(\frac{ah}{2}\right)^2 \sinh\left(\frac{bh}{2}\right)^2}{3},
\end{aligned} \tag{A.10}$$

$$\begin{aligned}
D = & 8 \cosh\left(\frac{ah}{2}\right) \sinh\left(\frac{bh}{2}\right) - \frac{2Rr \cosh\left(\frac{ah}{2}\right) \sinh\left(\frac{bh}{2}\right)}{3} \\
& - 8 \cosh\left(\frac{ah}{2}\right)^2 \cosh\left(\frac{bh}{2}\right) \sinh\left(\frac{bh}{2}\right) \\
& + \frac{Rr \cosh\left(\frac{ah}{2}\right)^2 \cosh\left(\frac{bh}{2}\right) \sinh\left(\frac{bh}{2}\right)}{3} + \frac{16Pe \sinh\left(\frac{ah}{2}\right) \sinh\left(\frac{bh}{2}\right)}{3} \\
& - \frac{8Pe \cosh\left(\frac{ah}{2}\right) \cosh\left(\frac{bh}{2}\right) \sinh\left(\frac{ah}{2}\right) \sinh\left(\frac{bh}{2}\right)}{3} \\
& - 8 \cosh\left(\frac{bh}{2}\right) \sinh\left(\frac{ah}{2}\right)^2 \sinh\left(\frac{bh}{2}\right) \\
& + \frac{Rr \cosh\left(\frac{bh}{2}\right) \sinh\left(\frac{ah}{2}\right)^2 \sinh\left(\frac{bh}{2}\right)}{3},
\end{aligned} \tag{A.11}$$

$$\begin{aligned}
E = & 2 - \frac{Rr}{3} - \frac{2Rr \cosh\left(\frac{ah}{2}\right) \cosh\left(\frac{bh}{2}\right)}{3} - 2 \cosh\left(\frac{ah}{2}\right)^2 \cosh\left(\frac{bh}{2}\right)^2 \\
& + \frac{8Pe \cosh\left(\frac{bh}{2}\right) \sinh\left(\frac{ah}{2}\right)}{3} + \frac{4Pe \cosh\left(\frac{ah}{2}\right) \cosh\left(\frac{bh}{2}\right)^2 \sinh\left(\frac{ah}{2}\right)}{3} \\
& - 2 \cosh\left(\frac{bh}{2}\right)^2 \sinh\left(\frac{ah}{2}\right)^2 - 2 \cosh\left(\frac{ah}{2}\right)^2 \sinh\left(\frac{bh}{2}\right)^2 \\
& + \frac{4Pe \cosh\left(\frac{ah}{2}\right) \sinh\left(\frac{ah}{2}\right) \sinh\left(\frac{bh}{2}\right)^2}{3} - 2 \sinh\left(\frac{ah}{2}\right)^2 \sinh\left(\frac{bh}{2}\right)^2,
\end{aligned} \tag{A.12}$$

$$\begin{aligned}
F = & 2 - \frac{Rr}{3} - \frac{2Rr \cosh\left(\frac{ah}{2}\right) \cosh\left(\frac{bh}{2}\right)}{3} - 2 \cosh\left(\frac{ah}{2}\right)^2 \cosh\left(\frac{bh}{2}\right)^2 \\
& + \frac{8Pe \cosh\left(\frac{bh}{2}\right) \sinh\left(\frac{ah}{2}\right)}{3} + \frac{4Pe \cosh\left(\frac{ah}{2}\right) \cosh\left(\frac{bh}{2}\right)^2 \sinh\left(\frac{ah}{2}\right)}{3} \\
& - 2 \cosh\left(\frac{bh}{2}\right)^2 \sinh\left(\frac{ah}{2}\right)^2 - 2 \cosh\left(\frac{ah}{2}\right)^2 \sinh\left(\frac{bh}{2}\right)^2
\end{aligned}$$

$$+ \frac{4Pe \cosh\left(\frac{ah}{2}\right) \sinh\left(\frac{ah}{2}\right) \sinh\left(\frac{bh}{2}\right)^2}{3} - 2 \sinh\left(\frac{ah}{2}\right)^2 \sinh\left(\frac{bh}{2}\right)^2. \quad (\text{A.13})$$

In the above,

$$a = \frac{u}{k}, \quad (\text{A.14})$$

$$b = \frac{\sqrt{u^2 - 4k\lambda^2}}{2k}. \quad (\text{A.15})$$

References

- [1] B. Ataie-Ashtiani, D.A. Lockington, R.E. Volker, Numerical correction of finite-difference solution of the advection–dispersion equation with reaction, *J. Cont. Hydrol.* 23 (1996) 149–156.
- [2] B.J. Noye, H.H. Tan, A third-order semi-implicit finite difference method for solving one-dimensional convection diffusion equation, *Int. J. Numer. Meth. Eng.* 26 (1988) 1615–1629.
- [3] Md. Akram Hossain, Modelling advective dispersive transport with reaction; an accurate explicit finite difference model, *Appl. Math. Comput.* 102 (1999) 101–108.
- [4] I. Harari, T.J.R. Hughes, Stabilized finite element methods for steady advection–diffusion with production, *Comput. Meth. Appl. Mech. Eng.* 115 (1994) 165–191.
- [5] Md. Akram Hossain, D.R. Yonge, On Galerkin models for transport in groundwater, *Appl. Math. Comput.* 109 (1999) 249–263.
- [6] Md. Akram Hossain, D.R. Yonge, Accuracy of the Taylor–Galerkin model for contaminant transport in groundwater, *Appl. Math. Comput.* 102 (1999) 109–119.
- [7] S. Idelsohn, N. Nigro, M. Storti, G. Buscaglia, A Petrov–Galerkin foundation for advection–reaction–diffusion problems, *Comput. Meth. Appl. Mech. Eng.* 136 (1996) 27–46.
- [8] R. Codina, Comparison of some finite element methods for solving the diffusion–convection–reaction equation, *Comput. Meth. Appl. Mech. Eng.* 156 (1998) 185–210.
- [9] T.J.R. Hughes, A.N. Brooks, A multi-dimensional upwind scheme with no crosswind diffusion, in: T.J.R. Hughes (Ed.), *Finite Element Methods for Convection Dominated Flows*, vol. 34, AMD ASME, New York, 1979, pp. 19–35.
- [10] R.F. Warming, B.J. Hyette, The modified equation approach to the stability and accurate analysis of finite-difference methods, *J. Comput. Phys.* 14 (1974) 159–179.
- [11] J.C. Tannehill, D.A. Anderson, R.H. Pletcher, *Computational Fluid Mechanics and Heat Transfer*, II ed., Taylor & Francis, Washington, 1997.
- [12] T. Meis, U. Marcowitz, Numerical solution of partial differential equations, *Appl. Math. Sci.* 22 (1981).
- [13] Oistein Bøe, A monotone Petrov–Galerkin method for quasilinear parabolic differential equations, *SIAM J. Sci. Comput.* 14 (5) (1993) 1057–1071.
- [14] A. Berman, R.J. Plemmons, *Nonnegative Matrices in the Mathematical Science*, Academic Press, New York, 1979.
- [15] A. Harten, High-resolution schemes for hyperbolic conservation laws, *J. Comput. Phys.* 49 (1983) 357–385.